Geophysical Research Letters

RESEARCH LETTER
10.1029/2022GL098839

The Internal Structure and Dynamics of Jupiter Unveiled by a High-Resolution Magnetic Field and Secular Variation Model

S. Sharan[1], B. Langlais[1], H. Amit[1], E. Thébault[2], M. Pinceloup[1], and O. Verhoeven[1]

[1]Laboratoire de Planétologie et Géosciences, CNRS UMR 6112, Nantes Université, Université d'Angers, Le Mans Université, Nantes, France, [2]Laboratoire Magma et Volcans, Université Clermont Auvergne, UMR 6524, CNRS, IRD, OPGC, Clermont-Ferrand, France

Key Points:

- Magnetic field of Jupiter is modeled from Juno's first 4 years of observations
- A degree 16 magnetic field model and degree 8 secular variation model are derived
- The model indicates a dynamo not far from the surface and complex motions deep inside Jupiter

Supporting Information:

Supporting Information may be found in the online version of this article.

Correspondence to:

S. Sharan and B. Langlais,
shivangi.sharan@univ-nantes.fr;
benoit.langlais@univ-nantes.fr

Citation:

Sharan, S., Langlais, B., Amit, H., Thébault, E., Pinceloup, M., & Verhoeven, O. (2022). The internal structure and dynamics of Jupiter unveiled by a high-resolution magnetic field and secular variation model. *Geophysical Research Letters*, *49*, e2022GL098839. https://doi.org/10.1029/2022GL098839

Received 28 MAR 2022
Accepted 21 JUL 2022

Abstract Unique information about the dynamo process acting at Jupiter can be inferred by modeling and interpreting its magnetic field. Using the fluxgate magnetometer measurements acquired during the 4 years of the Juno mission, we derive a magnetic field model which describes simultaneously the main field and the secular variation (SV) up to spherical harmonic degrees 16 and 8, respectively. Apart from the Earth's, this is the first time another planetary magnetic field along with its time variation is described to such a high degree. We use properties of the power spectrum of the static field to infer the upper boundary of the dynamo convective region at 0.830 ± 0.022 Jupiter radius. The SV and correlation times are relatively comparable to the Earth's and indicate that the field is dominated by advection. The field and SV morphologies suggest zonal as well as non-zonal deep fluid motions.

Plain Language Summary The interior of Jupiter can be described broadly as a dense core surrounded by fluids, dominantly hydrogen and helium. The hydrogen-rich metallic fluid generates the strongest planetary magnetic field in the Solar System. Modeling and interpreting this field gives essential information about the dynamo process inside Jupiter. We use the Juno mission data throughout 4 years (or, 28 orbits) to derive an internal magnetic field and secular variation (SV) model using spherical harmonic functions. We compute a magnetic field model to degree 16 for its static part, and model its temporal variation to degree 8. The power spectrum of the magnetic field model is used to investigate the radius of the dynamo region. We infer that the convective region has an upper boundary at 0.830 ± 0.022 Jupiter radius. The strength of the annual change of field is relatively comparable to the Earth's. The slope of the SV timescales indicates that the dynamo is dominated by advective effects. The SV displays a maximum near the equator with a bi-polar structure in agreement with zonal drift of the Great Blue Spot. However, numerous small scale SV structures suggest that the flow at the interior is complex involving both zonal and non-zonal features.

1. Introduction

The interior of the giant planets of our Solar System can be described in simple terms as consisting of a core of unknown composition surrounded by fluid envelopes (Guillot, 2005). For Jupiter, the core could be small and dense, but also large and dilute (Wahl et al., 2017). The overlying envelopes consist of an inner layer of metallic hydrogen and an outer layer of molecular hydrogen. Recent experimental results describe a transition H-He demixing layer, suggesting Helium rain between depths 0.68 and 0.84 R_J (Jupiter's equatorial radius, 1 R_J = 71,492 km) (Brygoo et al., 2021). The high temperature and pressure inside the planet renders it electrically conducting. Convection in the electrically conductive metallic hydrogen generates the strong Jovian magnetic field (Jones, 2011, 2014). In contrast to rocky bodies, Jupiter does not have an abrupt change between its metallic hydrogen (magnetic source) and molecular hydrogen (source free) regions. The change is expected to be gradual. The electrical conductivity profile of the different hydrogen layers at different depths from an ab-initio simulation (French et al., 2012) does not indicate a clear value of the dynamo region radius. Previous attempts to constrain this radius using the magnetic energy spectrum place it somewhere between 0.80 and 0.90 R_J (Connerney et al., 2022; Langlais et al., 2014; Tsang & Jones, 2020).

Jupiter's magnetic field has been measured by various flybys and orbiting satellites. The observations made by the flybys of Pioneer 10 and 11, Voyager 1 and 2 (during the seventies), and the Ulysses probe (early nineties) gave some initial information about the planet (Balogh et al., 1992; Ness et al., 1979; Smith et al., 1974). The first orbiting satellite, Galileo, was launched in 1989. It provided measurements from Jupiter and its moons from

1995 to 2003. Although these magnetic observations are spread over long periods of time, there have been only a few attempts to constrain or estimate the temporal variation of the field (Connerney et al., 1982; Ridley & Holme, 2016; Yu et al., 2010). Out of these studies, only Ridley and Holme (2016) co-estimated the secular variation (SV) with the main field (MF) using magnetic field measurements made between 1973 and 2003. However, due to the inhomogeneous temporal and geographical data distribution, most of the selected observations were from the Galileo mission at low latitudes. Ridley and Holme (2016) computed two models, one with only MF time averaged Gauss coefficients and one with time dependent MF and SV coefficients. The latter model was considered better because of its lower residuals and greater smoothness. Nevertheless, they considered their SV model to be reliable only up to degree 2.

None of these spacecrafts provided data near the poles. This was overcome by the recent Juno measurements. Juno space probe was launched on August 5, 2011 and entered Jupiter's orbit in July 2016. Its magnetic measurements have already been used to propose recent models of the Jovian field. Connerney et al. (2018) provided a spherical harmonic (SH) internal field model up to degree 10 using the first nine orbits. This initial model was improved by Connerney et al. (2022) who calculated a static model up to degree 30 for internal and degree 1 for external, from the first 33 orbits, using a generalized inversion technique to damp the unresolved parameters. They state that the Gauss coefficients are well resolved until degree 13 though useful information can be retained until degree 18 for some coefficients. Jupiter's internal field is characterized by a very high magnitude, showing both dipole and non-dipole parts. The non-dipole field is dominantly observed in the northern hemisphere. Field change over a 45-year time span was observed and zonal drift was invoked to explain the temporal change of an intense magnetic flux patch near the equator (Moore et al., 2018, 2019). An updated external magnetodisk field model for Juno is also available (Connerney et al., 2020). None of the existing models based on Juno data attempt to model explicitly the current global temporal variation of the field.

In this study, we use the high quality Juno measurements to derive a SH model of the Jovian field, simultaneously describing its MF and SV up to SH degrees 16 and 8, respectively. Section 2 details the data and the selection criteria we use for this study. Section 3 describes the method used to derive the models and their spectra that was assessed with a thorough synthetic analysis (Text S1 in Supporting Information S1). In Section 4 we analyze the model and discuss our results. We first determine the dynamo radius assuming white spectrum of specific parts of the field. We also calculate the SV correlation times of the Jovian field. We finally downward continue the field into Jupiter's interior to the estimated dynamo radius and infer kinematic properties. We conclude in Section 5.

2. Data

Juno has a near polar, highly elliptical orbit with apojove exceeding over 100 times Jupiter's radius. The prime mission lasted 5 years and provided data for 33 orbits with one complete orbit taking about 53 days. The space probe was initially planned to undergo a reduction maneuver for achieving 14-day science orbits but Juno entered safe mode for its second orbit, thereby remaining in its initial 53-day capture orbit for the entire mission. The spacecraft aims to obtain a global coverage of the planet. For the first eight orbits, the shift between successive orbits was 45° in longitude. The subsequent shifts reduce the longitudinal spacing by half to obtain data from the gaps left previously.

Juno uses two fluxgate magnetometers, located on one of the three solar arrays to measure the vector magnetic field. Magnetic field measurements acquired by Juno are available under two versions. The version 1 data provides measurements across the entire orbit, whereas the version 2 data gives only near planet measurements from the orbit, denoted as perijove hereafter. Both version 1 and 2 data are provided in three Cartesian coordinate systems—planetocentric, sun-state, and payload. Since planetocentric system is body-fixed, it is the most appropriate to study the internal field. We use the version 2 one-second data in planetocentric coordinates from the first 28 perijoves (data available for only 27 perijoves, excluding the second one). As discussed later, synthetic tests inversion including the latest perijoves from 29 to 33 leads to an increase in polar gaps that degrades some model coefficients. Perijove 19 was also dismissed because spurious oscillations were later observed.

The periapsis reaches altitude as low as 2,500 km, or radius 1.03 R_J, and precesses about 1° in latitude northward, starting from the equator, after each orbit. In order to minimize external field contributions and to increase the signal-to-noise ratio of high internal magnetic field harmonics, we select measurements near the planet's surface, that is, the vector data below an arbitrarily chosen altitude of 300,000 km (or radius $\sim 5.2R_J$). Moreover, due to

geometric attenuation with the altitude, high-altitude measurements are less sensitive to small spatial scales than the ones at comparatively lower altitudes. The vector data range from August 2016 to July 2020 giving 628,828 data locations, that are plotted in Figure S1 in Supporting Information S1. Minimum measured field intensity is of the order of 3,000 nT at maximum altitude while the maximum intensity reaches above 10^6 nT.

3. Methodology

The magnetic field in a source free location can be expressed as the gradient of a scalar potential V that satisfies the Laplace equation:

$$\nabla^2 V = 0 \tag{1}$$

The potential for internal and external sources can be written as an expansion of SH functions:

$$\begin{aligned} V(r,\theta,\phi,t) = R_J \sum_{n=1}^{n_i^{\max}} \sum_{m=0}^{n} \left\{ \left(\frac{R_J}{r}\right)^{n+1} \left(g_n^m(t)\cos m\phi + h_n^m(t)\sin m\phi\right) P_n^m(\cos\theta) \right\} \\ + R_J \sum_{n=1}^{n_e^{\max}} \sum_{m=0}^{n} \left\{ \left(\frac{r}{R_J}\right)^{n} \left(q_n^m(t)\cos m\phi + s_n^m(t)\sin m\phi\right) P_n^m(\cos\theta) \right\} \end{aligned} \tag{2}$$

where (r, θ, ϕ, t) are the planetocentric spherical coordinates (radius, co-latitude, and longitude) and time, respectively. R_J is the reference radius equal to Jupiter's equatorial radius (71,492 km). $g_n^m(t)$ and $h_n^m(t)$ are the time-dependent internal field Gauss coefficients of degree n and order m while $q_n^m(t)$ and $s_n^m(t)$ are the external field coefficients. P_n^m are the Schmidt quasi-normalized associated Legendre functions. $n_i^{\max}$ and $n_e^{\max}$ are the maximum degree for the internal and external field coefficients, respectively.

To calculate the SH coefficients, we apply a weighted least-squares inversion approach based on a singular value decomposition algorithm. The weights are defined in nT by the instrument error and intrinsic noise for each Juno data location (Connerney et al., 2017). The temporal variation of the internal field is calculated using B-splines of order 2, which are piece-wise polynomials describing the time derivatives between defined knots. We use three knots, at the beginning, middle, and final epoch of the measurements (spacing is about 1.95 years). This parameterization was extensively tested on the selected set of Juno's data location with a synthetic time-varying internal magnetic field mimicking the strength and the power spectrum of the actual internal field of Jupiter. The inversion on synthetic measurements does not require regularization with this parameterization and it is stable with random noise (Details of the method, tests, and assessments are provided in Text S1 in Supporting Information S1).

Once the Gauss coefficients and their time variation are estimated, several statistical quantities can be computed. The Lowes-Mauersberger spectrum represents the magnetic field power spectrum per SH degree (Lowes, 2007; Mauersberger, 1956). For a given time, and at a given radius r, it can be defined as

$$\mathcal{R}_n = (n+1)\left(\frac{R_J}{r}\right)^{(2n+4)} \sum_{m=0}^{n} \left[(g_n^m)^2 + (h_n^m)^2\right] \tag{3}$$

at SH degree n. Similarly, for the SV, it can be defined as

$$\mathcal{S}_n = (n+1)\left(\frac{R_J}{r}\right)^{(2n+4)} \sum_{m=0}^{n} \left[(\dot{g}_n^m)^2 + \left(\dot{h}_n^m\right)^2\right] \tag{4}$$

where $\dot{g}_n^m$ and $\dot{h}_n^m$ are the Gauss coefficients of the SV.

The MF and its spectrum $\mathcal{R}_n$ can be upward or downward continued, provided there are no magnetic field sources present in between. This property has been used to derive estimates of the radius of the dynamo region, or of the liquid core, in the case of the Earth. This is also known as the white noise hypothesis: immediately outside the dynamo region, the part of the magnetic spectrum associated with the dynamo is assumed flat, and the depth to the dynamo can thus be grossly estimated (Lowes, 1974). However some terms ($n = 1$ and $n = 2$) have to be ignored in order for this approximation to match the radius of the Earth's core (Cain et al., 1989; Voorhies, 2004). Langlais et al. (2014) found that certain parts of the spectrum $\mathcal{R}_n$, namely the non-zonal and quadrupole families, are independent of n at some radius r (see Text S2 in Supporting Information S1, for details). On Earth, these

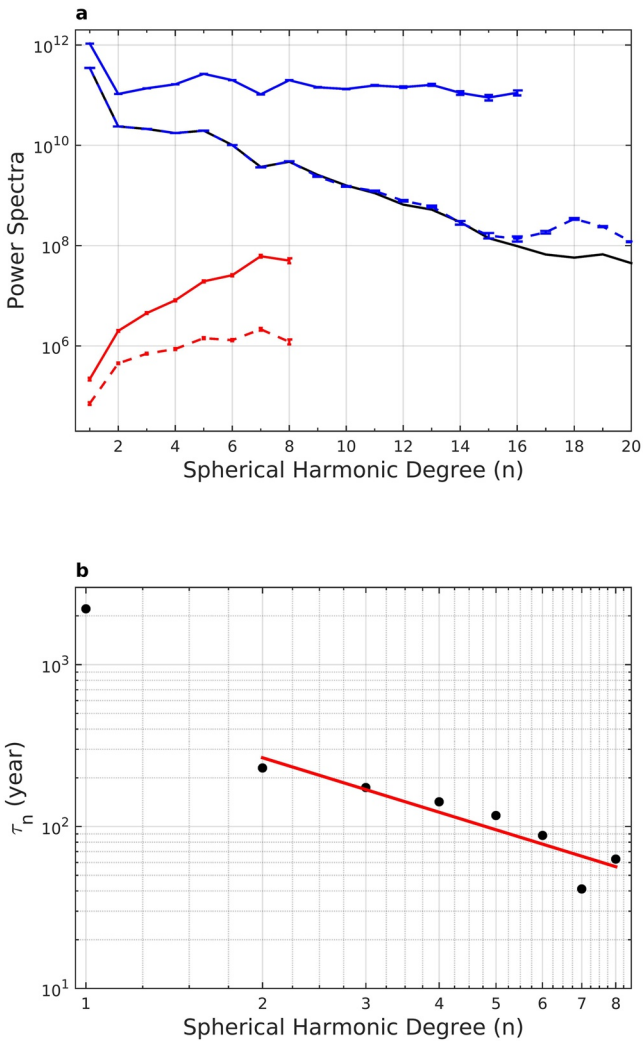

Figure 1. (a) The power spectra with error bars for the main field (shown in blue, units - nT^2) and secular variation (shown in red, units - $(nT/year)^2$) of the model at the surface (dashed line) and at $\mathbf{R}_{sf}$ (solid line). The main field terms for $n > 16$ are not downward continued to $\mathbf{R}_{sf}$. The black line is the main field power spectrum of the model of Connerney et al. (2022), which lies within the 99% bound of our model. (b) The secular variation timescales of the model. The red line is the linear best fit to the non-dipole part.

approaches return the value of the core or dynamo radius with a combined relative error lower than 0.3%. In the following, we refer to the dynamo radius at Jupiter, estimated from the non-zonal and quadrupole families of coefficients, as $\mathbf{R}_{sf}$. It can be interpreted as the radius of the top of the source region, or the bottom of the source free region.

The correlation times as a function of degree n can also be defined combining the quantities $\mathcal{R}_n$ and $\mathcal{S}_n$. The correlation times, also referred to as the SV timescales, give a measure of how long it takes for the field of a particular degree to get reorganized, or become uncorrelated to its former state at that degree (Amit et al., 2018; Christensen & Tilgner, 2004; Hulot & Le Mouël, 1994). It is expressed as

$$\tau_n = \sqrt{\frac{\mathcal{R}_n}{\mathcal{S}_n}} \tag{5}$$

4. Results and Discussion

We calculate the MF model up to degree 20 and the SV to degree 8. The external field is estimated up to degree 2. Suspicion of power leakage from unresolved small and rapid spatial scales leads us to reject 29 out of the 608 eigenvalues in the weighted least-squares inversion. As a consequence, the terms beyond SH degree 16 are damped, and the final model is truncated to $n_i^{\max} = 16$. We estimate a posteriori standard error on the coefficients from the covariance matrix and the inversion misfit for the three vector components. The misfits for each vector component are given in Table S1 in Supporting Information S1. This table also shows the statistics for a model to SH degree 20 derived without SV. The misfit difference between these two cases supports the fact that a statistically significant and global SV is present in the measurements. The SV improves data fit better than increasing field complexity (see Ridley and Holme (2016) for a similar conclusion). Note that Connerney et al. (2022) also indicates strong evidences for local SV in the vicinity of Jupiter's Great Blue Spot between Juno perijoves 9 and 33. Figure 1a displays the MF (and the SV) power spectra with the 99% error bars. For comparison, the power spectrum of the model of Connerney et al. (2022) is also shown, which falls within the error bars down to SH degree 15–16. The increase of the power between $n = 16$ and 18 of our model probably arises because of the spectral aliasing of remaining signal in the measurements. We also note that with increasing orbits the satellite goes lower in altitude near the north pole while increasing the size of a gap at similar latitude ranges over the south pole area. This results in high degree, low order terms being less resolved (i.e., zonal and near zonal terms). Figure S2 in Supporting Information S1 shows the root mean square differences between Juno's dataset and predictions by our model, a model calculated without SV, and the model by Connerney et al. (2022), considering different truncation degrees for each model. At SH degree 16, our model and the model by Connerney et al. (2022) have a root mean square misfit to data equal to about 800 nT.

4.1. Inferences on the Internal Structure

We estimate the dynamo radius $\mathbf{R}_{sf}$ for varying truncation degrees of the MF model $n_i^{\max}$ seeking in a minimum least-squares sense the depth at which the power spectra from the non-zonal ($m \neq 0$) and quadrupole ($n + m$ even) families of coefficients are statistically flat (Langlais et al., 2014). The error bars on the estimated dynamo radius decrease up to truncation degree $n_i^{\max} = 16$ for both families (Figure S8 in Supporting Information S1). It is also the truncation degree for which the maximum likelihood estimates from the non-zonal and quadrupole families of power spectra coincide. This again supports the choice of truncating the present model to the maximum

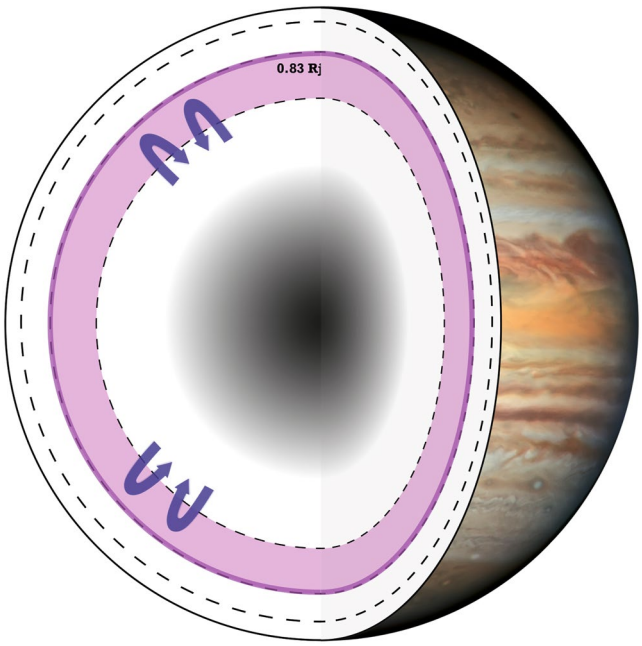

Figure 2. Schematic view of the interior of Jupiter. The bold violet line depicts our result $\mathbf{R}_{sf}$. The gray area depicts the core (0.2 R_J) and the possible dilute core region (Wahl et al., 2017; Wicht & Gastine, 2020). The violet area between the dotted lines (0.68 and 0.84 R_J) depicts the H-He phase separated layer (Brygoo et al., 2021). The top dotted line at 0.95 R_J depicts the depth where the jets decay down to the minimum (Kaspi et al., 2018). The arrows represent possible convection area with unknown origin depth.

degree 16. The maximum likelihood value from the non-zonal field is equal to 0.831 R_J and that from the quadrupole family is equal to 0.829 R_J. We use their mean and combine their standard errors to provide a single estimate for $R_{sf} = 0.830 \pm 0.022$ R_J. Previous studies such as the one by Connerney et al. (2018) estimate the dynamo radius "near 0.85 R_J" while Connerney et al. (2022) estimate it to $0.81R_J$ and Tsang and Jones (2020) between 0.82 and $0.87R_J$ using a numerical model. However, all these studies use the white noise hypothesis as discussed above, which ignores the $n = 1$ and even $n = 2$ terms.

For a dynamo to exist in a planet, two main criteria are required: an electrically conducting fluid and an energy source, which is often convection within a spherical shell in rotation. For Jupiter, the metallic hydrogen is the fluid, and its convective motion drives the dynamo. Convection can also take place in the source free region, without contributing to the dynamo. Wicht and Gastine (2020), through numerical simulations, suggested the possibility of two distinct dynamo regions inside Jupiter. The primary region would be at depth, and is responsible for the dipole dominated field geometry. The secondary one would be shallower, and operates where the equatorial jets encounter conductive material in the transition layer. However, surface jets motion decays rapidly with depth and are unlikely to extend at depths larger than about 3,000–3,500 km or ~0.95 R_J (Guillot et al., 2018; Kaspi et al., 2018). Christensen et al. (2020) suggested that a stratified layer, close to the surface, could quench the jets at depth and play a role in the secondary dynamo. Our study points toward a source free region extending deeper, with a radius placed at 0.830 R_J. This radius could correspond to the upper limit of the dynamo region. We note that it also matches well the radius of the transition layer in between the metallic and molecular hydrogen (Brygoo et al., 2021), rendering this layer part of the dynamo region (Figure 2). Our results do not provide constraints on the bottom radius of the dynamo and do not indicate a shallower secondary dynamo (Gastine & Wicht, 2021) above 0.830 R_J.

4.2. SV Timescales

The SV timescales are shown in Figure 1b. For Earth, the correlation time for the dipole is around 1,000 years and the lowest value at $\sim n_i^{\max} = 13$ is of the order of 10 years. Field models and numerical dynamo simulations indicate that the non-dipole SV timescales are inversely proportional to the SH degree (e.g., Bouligand et al., 2016; Lhuillier et al., 2011). For Jupiter, the correlation time for the dipole (τ_1) is 2,210 years while the lowest value we obtain is 40 years for degree 7. We observe similar inverse proportionality for the Jovian SV timescales. The best fit slope for $n = 2 - 8$ is -1.12 with a standard deviation of 0.21. According to the scaling theory of the magnetic induction equation, a slope of -1 corresponds to advective SV, whereas -2 indicates diffusive SV (Christensen et al., 2012; Holme & Olsen, 2006). A -2 slope for our model is well outside 2 standard deviations and can be excluded. Therefore, our best fit value -1.12 ± 0.21 suggests that the field change is dominated by advective effects, as is the case for Earth (Christensen et al., 2012; Lhuillier et al., 2011). In addition, the overall similarity between the non-dipole SV timescales of Jupiter and Earth suggests a similar magnetic Reynolds number (Christensen & Tilgner, 2004), that is, $Rm_J \sim 1{,}000$. In contrast, Wicht et al. (2019) concluded that diffusive effects might govern the dynamo in the transition layer. Though their transition region starts above $\mathbf{R}_{sf}$, the SV timescales we compute are independent of the radius, hence challenging the importance of diffusion. It thus remains an open question as to what phenomenon drives the observed SV of Jupiter.

4.3. Implications to Jupiter's Dynamo

Using the four morphological criteria defined in Christensen et al. (2010) for Earth-like dynamo models at the core-mantle boundary, we compare our results with the geodynamo. For comparison purposes, we set $n_i^{\max} = 8$ to calculate the different criteria, that is, smaller than that shown in Figures 3a–3f. The relative axial dipole power

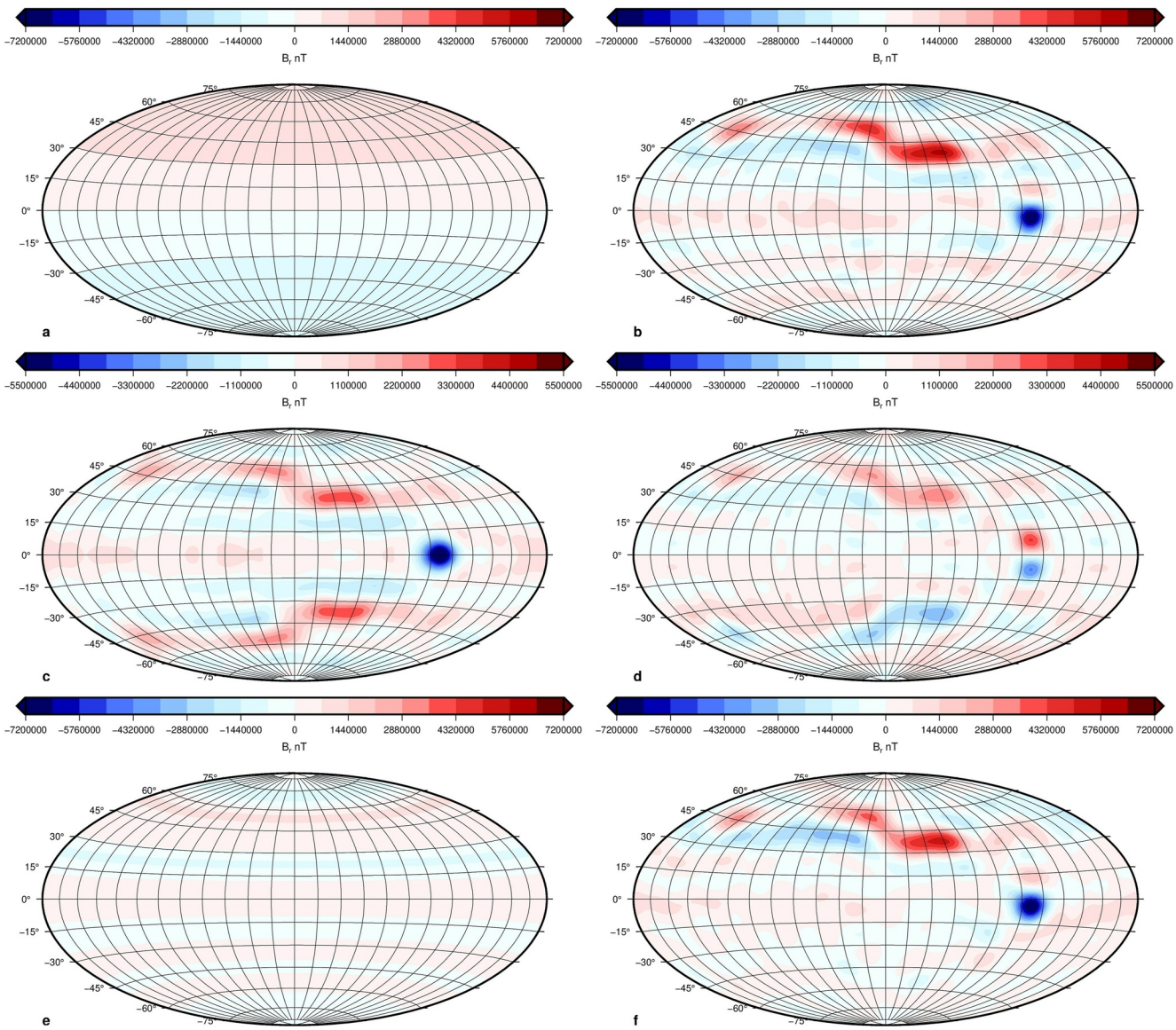

Figure 3. The radial field at $\mathbf{R}_{sf}$. (a) Axial dipole field. (b) Non-axial dipole field. (c) Non-dipole symmetric field. (d) Non-dipole anti-symmetric field. (e) Non-dipole zonal field. (f) Non-dipole non-zonal field. The maps are centered at 180° longitude.

for our model is 0.86 at $\mathbf{R}_{sf}$ while the standard value for Earth is 1.4, though the present-day value is about 1. This indicates that Jupiter's dynamo is either less dipolar or comparable to Earth's (Figures 3a and 3b). The equatorial anti-symmetry for Earth is 1.0, whereas our model provides a value of 0.52. A random equipartitioned non-dipole field ratio would give an equatorial anti-symmetry of 0.83 (Christensen et al., 2010). Thus, Jupiter's non-dipole field is more symmetric with respect to the equator than Earth's (Figures 3c and 3d). The zonal to non-zonal ratio for a random equipartitioned field is 0.10 (Christensen et al., 2010). For Earth, the value is 0.15, while for our model the value is 0.20, which indicates a stronger zonal contribution (Figures 3e and 3f). Lastly, the flux concentration for a purely dipole field is 0.8 and that for the geomagnetic field is 1.50 (Christensen et al., 2010). The flux concentration is considered low when flux exits one hemisphere and enters through the other uniformly. Conversely, it is large when it exits from a concentrated spot and enters the rest of the sphere uniformly. The concentration value for our model is 4.23. This very large value reflects the dominance of the large intense flux patch in the northern hemisphere.

Figure 4 shows the radial magnetic field and SV maps calculated using the model at Jupiter's surface and at $\mathbf{R}_{sf}$. The large positive radial field patch in the northern hemisphere and the intense negative patch near the equator

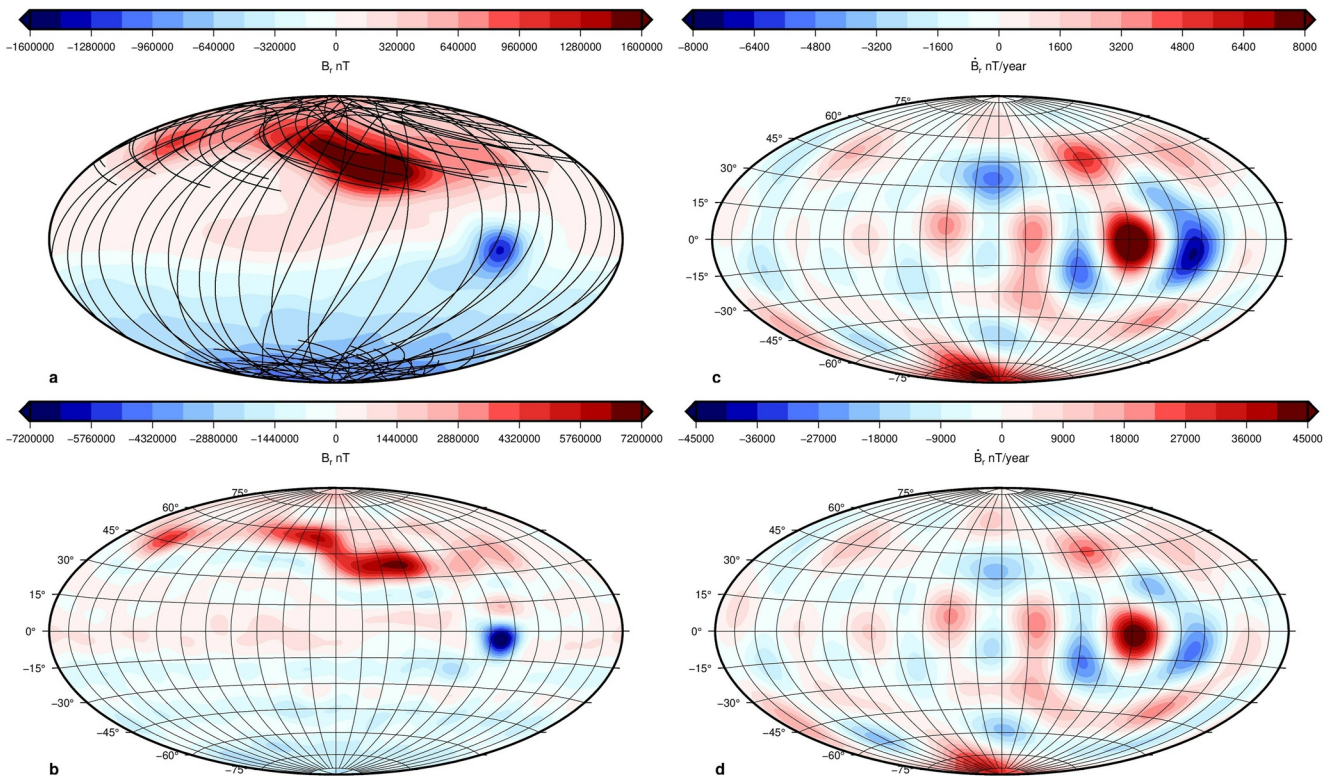

Figure 4. The (a, b) radial field and (c, d) its secular variation at (top) Jupiter's surface and (bottom) $\mathbf{R}_{sf}$. The maps are centered at 180° longitude. The lines in (a) show the orbit paths of the used data set.

(the Great Blue Spot) become more concentrated with depth. SV is of the order of 10^4 nT/year at the surface. This corresponds to a 2.3% change over the course of 4 years of the dataset used, compared to the 1.4% change over a similar duration for the Earth's magnetic field. As for Earth's, it should not be ignored when modeling the magnetic field over periods exceeding a few years.

The spatial pattern of temporal variation of the field brings further dynamical constraints. The power spectrum of the SV calculated at $\mathbf{R}_{sf}$ increases with degree (Figure 1a). Indeed, the SV reveals intense small scale structures (Figure 4). The strong negative radial field patch immediately south of the equator (Figure 4b) coincides with a pair of SV structures (Figure 4d), suggesting eastward drift (Amit, 2014; Livermore et al., 2017). This is opposite to the westward drifting low- and mid-latitude patches observed with Earth's SV (Aubert & Finlay, 2019; Bullard et al., 1950; Finlay & Jackson, 2003). This eastward drift could relate to the zonal winds observed at the surface or until 0.95 R_J (Moore et al., 2019). However, our model presents also other prominent SV structures which cannot be explained by zonal winds. There is some suggestion for a weak eastward drift near 45°N latitude, which is the center of the large positive radial field patch (Figure 4b). But, it is not associated with particularly strong SV for most of its structure, possibly indicating a region with dominantly field-aligned flow (Finlay & Amit, 2011). Livermore et al. (2017) gave similar explanation for the absence of strong SV at southern high latitudes of Earth. The southern hemisphere has many alternating sign SV patches up to 60°S latitude (Figure 4d) which are not correlated with particularly strong field structures (Figure 4b). Bearing in mind that the model is less constrained at the south pole, the opposite signs of B_r and $\dot{B}_r$ (Figure S3 in Supporting Information S1) suggest local fluid upwelling (Amit, 2014), similar to the field and SV below Earth's poles and in agreement with a classic meridional circulation inside the tangent cylinder (Cao et al., 2018; Olson & Aurnou, 1999). We note that the radial field and its SV from $\mathbf{R}_{sf}$ to the surface are weakly sensitive to depth (Figure 4), making these kinematic interpretations robust.

5. Concluding Remarks

We present a co-estimated magnetic field and SV model robust up to degree 16 and degree 8, respectively. The model uses Juno measurements made during the first 28 orbits. As expected, our static field resembles previously published field models (e.g., Connerney et al., 2022). However, we also present here for the first time a small-scale SV model for Jupiter. Our innovative Jovian magnetic SV model provides crucial insight into its deep interior and dynamics. We use two different families of the magnetic spectra and derive a consistent dynamo radius at 0.830 R_J. This confirms that the transition region is part of the dynamo generation. The SV allows to calculate SV timescales and leads to kinematic interpretations of inductive effects (Amit, 2014). The dominance of advective SV and the dipole SV timescale of Jupiter exhibit similarities with the geodynamo. The SV is consistent with zonal as well as non-zonal motions deep inside Jupiter. We further conclude that the global SV is significant and cannot be neglected over the course of 1 year or so.

More insights into the dynamo regime could be gleaned by inferring the flow at Jupiter's deep interior. Our field and SV model can be inverted for the flow at $\mathbf{R}_{sf}$. Such an inversion, which is commonly performed for the flow at the top of Earth's core (Holme, 2015), was performed for Jupiter by Ridley and Holme (2016), but using a very low resolution SV model. More data are also needed to increase the resolution of the field model and to confirm the temporal variation observed during the last 4 years. This will come from Juno during the upcoming extended mission, but also when the ESA's JUICE mission enters Jupiter's orbit at the end of this decade.

Data Availability Statement

All Juno magnetometer data used here are publicly available on NASA's Planetary Data System (PDS) at Planetary Plasma Interactions (PPI) node at https://pds-ppi.igpp.ucla.edu/search/?sc=Juno%26t=Jupiter%26i=FGM. The model coefficients and their standard deviation for the static field to degree 16 and its SV to degree 8 are available at: https://doi.org/10.5281/zenodo.6564162.

Acknowledgments
This work was financially supported by the Centre National D'Études Spatiales (CNES). The authors would like to thank the Editor, Andrew Dombard, and two anonymous reviewers for their useful comments which contributed to improving the manuscript. We thank Stéphanie Beaunay for graphical assistance. We acknowledge AGU's data policy.

References

Amit, H. (2014). Can downwelling at the top of the earth's core be detected in the geomagnetic secular variation? *Physics of the Earth and Planetary Interiors*, *229*, 110–121. https://doi.org/10.1016/j.pepi.2014.01.012

Amit, H., Coutelier, M., & Christensen, U. R. (2018). On equatorially symmetric and antisymmetric geomagnetic secular variation timescales. *Physics of the Earth and Planetary Interiors*, *276*, 190–201. (Special Issue:15th SEDI conference). https://doi.org/10.1016/j.pepi.2017.04.009

Aubert, J., Finlay, C. C., & Fournier, A. (2013). Bottom-up control of geomagnetic secular variation by the earth's inner core. *Nature*, *502*(7470), 219–223. https://doi.org/10.1038/nature12574

Balogh, A., Dougherty, M. K., Forsyth, R. J., Southwood, D. J., Smith, E. J., Tsurutani, B. T., et al. (1992). Magnetic field observations during the Ulysses flyby of Jupiter. *Science*, *257*(5076), 1515–1518. https://doi.org/10.1126/science.257.5076.1515

Bouligand, C., Gillet, N., Jault, D., Schaeffer, N., Fournier, A., & Aubert, J. (2016). Frequency spectrum of the geomagnetic field harmonic coefficients from dynamo simulations. *Geophysical Journal International*, *207*(2), 1142–1157. https://doi.org/10.1093/gji/ggw326

Brygoo, S., Loubeyre, P., Millot, M., Rygg, J. R., Celliers, P. M., Eggert, J. H., et al. (2021). Evidence of hydrogen-helium immiscibility at Jupiter-interior conditions. *Nature*, *593*(7860), 517–521. https://doi.org/10.1038/s41586-021-03516-0

Bullard, E. C., Freedman, C., Gellman, H., & Nixon, J. (1950). The westward drift of the earth's magnetic field. *Philosophical Transactions of the Royal Society of London - Series A: Mathematical and Physical Sciences*, *243*(859), 67–92. https://doi.org/10.1098/rsta.1950.0014

Cain, J. C., Wang, Z., Schmitz, D. R., & Meyer, J. (1989). The geomagnetic spectrum for 1980 and core-crustal separation. *Geophysical Journal International*, *97*(3), 443–447. https://doi.org/10.1111/j.1365-246X.1989.tb00514.x

Cao, H., Yadav, R. K., & Aurnou, J. M. (2018). Geomagnetic polar minima do not arise from steady meridional circulation. *Proceedings of the National Academy of Sciences*, *115*(44), 11186–11191. https://doi.org/10.1073/pnas.1717454115

Christensen, U. R., Aubert, J., & Hulot, G. (2010). Conditions for earth-like geodynamo models. *Earth and Planetary Science Letters*, *296*(3), 487–496. https://doi.org/10.1016/j.epsl.2010.06.009

Christensen, U. R., & Tilgner, A. (2004). Power requirement of the geodynamo from ohmic losses in numerical and laboratory dynamos. *Nature*, *429*(6988), 169–171. https://doi.org/10.1038/nature02508

Christensen, U. R., Wardinski, I., & Lesur, V. (2012). Timescales of geomagnetic secular acceleration in satellite field models and geodynamo models. *Geophysical Journal International*, *190*(1), 243–254. https://doi.org/10.1111/j.1365-246X.2012.05508.x

Christensen, U. R., Wicht, J., & Dietrich, W. (2020). Mechanisms for limiting the depth of zonal winds in the gas giant planets. *The Astrophysical Journal*, *890*(1), 61. https://doi.org/10.3847/1538-4357/ab698c

Connerney, J. E. P., Acuña, M. H., & Ness, N. F. (1982). Voyager 1 assessment of Jupiter's planetary magnetic field. *Journal of Geophysical Research*, *87*(A5), 3623–3627. https://doi.org/10.1029/JA087iA05p03623

Connerney, J. E. P., Benn, M., Bjarno, J. B., Denver, T., Espley, J., Jorgensen, J. L., et al. (2017). The juno magnetic field investigation. *Space Science Reviews*, *213*(1), 39–138. https://doi.org/10.1007/s11214-017-0334-z

Connerney, J. E. P., Kotsiaros, S., Oliversen, R. J., Espley, J. R., Joergensen, J. L., Joergensen, P. S., et al. (2018). A new model of Jupiter's magnetic field from juno's first nine orbits. *Geophysical Research Letters*, *45*(6), 2590–2596. https://doi.org/10.1002/2018GL077312

Connerney, J. E. P., Timmins, S., Herceg, M., & Joergensen, J. L. (2020). A Jovian magnetodisc model for the juno era. *Journal of Geophysical Research: Space Physics*, *125*(10), e2020JA028138. https://doi.org/10.1029/2020JA028138

Connerney, J. E. P., Timmins, S., Oliversen, R. J., Espley, J. R., Joergensen, J. L., Kotsiaros, S., et al. (2022). A new model of Jupiter's magnetic field at the completion of Juno's prime mission. *Journal of Geophysical Research: Planets*, *127*(2), e2021JE007055. https://doi.org/10.1029/2021JE007055

Finlay, C. C., & Amit, H. (2011). On flow magnitude and field-flow alignment at Earth's core surface. *Geophysical Journal International*, *186*(1), 175–192. https://doi.org/10.1111/j.1365-246X.2011.05032.x

Finlay, C. C., & Jackson, A. (2003). Equatorially dominated magnetic field change at the surface of earth's core. *Science*, *300*(5628), 2084–2086. Retrieved from https://science.sciencemag.org/content/300/5628/2084. https://doi.org/10.1126/science.1083324

French, M., Becker, A., Lorenzen, W., Nettelmann, N., Bethkenhagen, M., Wicht, J., & Redmer, R. (2012). Ab initio simulations for material properties along the Jupiter adiabat. *The Astrophysical Journal - Supplement Series*, *202*(1), 5. https://doi.org/10.1088/0067-0049/202/1/5

Gastine, T., & Wicht, J. (2021). Stable stratification promotes multiple zonal jets in a turbulent Jovian dynamo model. *Icarus*, *368*, 114514. Retrieved from https://www.sciencedirect.com/science/article/pii/S0019103521001895. https://doi.org/10.1016/j.icarus.2021.114514

Guillot, T. (2005). The interiors of giant planets: Models and outstanding questions. *Annual Review of Earth and Planetary Sciences*, *33*(1), 493–530. https://doi.org/10.1146/annurev.earth.32.101802.120325

Guillot, T., Miguel, Y., Militzer, B., Hubbard, W. B., Kaspi, Y., Galanti, E., et al. (2018). A suppression of differential rotation in Jupiter's deep interior. *Nature*, *555*(7695), 227–230. https://doi.org/10.1038/nature25775

Holme, R. (2015). Large-scale flow in the core. In *Treatise on geophysics* (pp. 91–113). https://doi.org/10.1016/B978-0-444-53802-4.00138-X

Holme, R., & Olsen, N. (2006). Core surface flow modelling from high-resolution secular variation. *Geophysical Journal International*, *166*(2), 518–528. https://doi.org/10.1111/j.1365-246X.2006.03033.x

Hulot, G., & Le Mouël, J. (1994). A statistical approach to the earth's main magnetic field. *Physics of the Earth and Planetary Interiors*, *82*(3), 167–183. Retrieved from https://www.sciencedirect.com/science/article/pii/0031920194900701. https://doi.org/10.1016/0031-9201(94)90070-1

Jones, C. A. (2011). Planetary magnetic fields and fluid dynamos. *Annual Review of Fluid Mechanics*, *43*(1), 583–614. https://doi.org/10.1146/annurev-fluid-122109-160727

Jones, C. A. (2014). A dynamo model of Jupiter's magnetic field. *Icarus*, *241*, 148–159. Retrieved from https://www.sciencedirect.com/science/article/pii/S0019103514003315. https://doi.org/10.1016/j.icarus.2014.06.020

Kaspi, Y., Galanti, E., Hubbard, W. B., Stevenson, D. J., Bolton, S. J., Iess, L., et al. (2018). Jupiter's atmospheric jet streams extend thousands of kilometres deep. *Nature*, *555*(7695), 223–226. https://doi.org/10.1038/nature25793

Langlais, B., Amit, H., Larnier, H., Thébault, E., & Mocquet, A. (2014). A new model for the (geo)magnetic power spectrum, with application to planetary dynamo radii. *Earth and Planetary Science Letters*, *401* , 347–358. https://doi.org/10.1016/j.epsl.2014.05.013

Lhuillier, F., Fournier, A., Hulot, G., & Aubert, J. (2011). The geomagnetic secular-variation timescale in observations and numerical dynamo models. *Geophysical Research Letters*, *38*(9). Retrieved from https://agupubs.onlinelibrary.wiley.com/doi/abs/10.1029/2011GL047356. https://doi.org/10.1029/2011GL047356

Livermore, P. W., Hollerbach, R., & Finlay, C. C. (2017). An accelerating high-latitude jet in earth's core. *Nature Geoscience*, *10*(1), 62–68. https://doi.org/10.1038/ngeo2859

Lowes, F. J. (1974). Spatial power spectrum of the main geomagnetic field, and extrapolation to the core. *Geophysical Journal International*, *36*(3), 717–730. https://doi.org/10.1111/j.1365-246X.1974.tb00622.x

Lowes, F. J. (2007). Geomagnetic spectrum, spatial. In D. Gubbins & E. Herrero-Bervera (Eds.), *Encyclopedia of geomagnetism and paleomagnetism* (pp. 350–353). Dordrecht: Springer Netherlands. https://doi.org/10.1007/978-1-4020-4423-6_126

Mauersberger, P. (1956). Das mittel der energiedichte des geomagnetischen hauptfeldes an der erdoberflache und seine saulare anderung. *Gerlands Beitr. Geophys.*, *65*, 207–215. Retrieved from https://ci.nii.ac.jp/naid/10006217427/en/

Moore, K. M., Cao, H., Bloxham, J., Stevenson, D. J., Connerney, J. E. P., & Bolton, S. J. (2019). Time variation of Jupiter's internal magnetic field consistent with zonal wind advection. *Nature Astronomy*, *3*(8), 730–735. https://doi.org/10.1038/s41550-019-0772-5

Moore, K. M., Yadav, R. K., Kulowski, L., Cao, H., Bloxham, J., Connerney, J. E. P., et al. (2018). A complex dynamo inferred from the hemispheric dichotomy of Jupiter's magnetic field. *Nature*, *561*(7721), 76–78. https://doi.org/10.1038/s41586-018-0468-5

Ness, N. F., Acuna, M. H., Lepping, R. P., Burlaga, L. F., Behannon, K. W., & Neubauer, F. M. (1979). Magnetic field studies at Jupiter by voyager 1: Preliminary results. *Science*, *204*(4396), 982–987. https://doi.org/10.1126/science.204.4396.982

Olson, P., & Aurnou, J. (1999). A polar vortex in the earth's core. *Nature*, *402*(6758), 170–173. https://doi.org/10.1038/46017

Ridley, V. A., & Holme, R. (2016a). Modeling the Jovian magnetic field and its secular variation using all available magnetic field observations. *Journal of Geophysical Research: Planets*, *121*(3), 309–337. Retrieved from https://agupubs.onlinelibrary.wiley.com/doi/abs/10.1002/2015JE004951. https://doi.org/10.1002/2015je004951

Smith, E. J., Davis, L., Jr., Jones, D. E., Coleman, P. J., Jr., Colburn, D. S., Dyal, P., et al. (1974). The planetary magnetic field and magnetosphere of Jupiter: Pioneer 10. *Journal of Geophysical Research*, *79*(25), 3501–3513. Retrieved from https://agupubs.onlinelibrary.wiley.com/doi/abs/10.1029/JA079i025p03501. https://doi.org/10.1029/ja079i025p03501

Tsang, Y.-K., & Jones, C. A. (2020). Characterising Jupiter's dynamo radius using its magnetic energy spectrum. *Earth and Planetary Science Letters*, *530*, 115879. Retrieved from https://www.sciencedirect.com/science/article/pii/S0012821X19305710. https://doi.org/10.1016/j.epsl.2019.115879

Voorhies, C. V. (2004). Narrow-scale flow and a weak field by the top of earth's core: Evidence from Ørsted, Magsat, and secular variation. *Journal of Geophysical Research*, *109*(B3). Retrieved from https://agupubs.onlinelibrary.wiley.com/doi/abs/10.1029/2003JB002833. https://doi.org/10.1029/2004jb003289

Wahl, S. M., Hubbard, W. B., Militzer, B., Guillot, T., Miguel, Y., Movshovitz, N., et al. (2017). Comparing Jupiter interior structure models to *Juno* gravity measurements and the role of a dilute core. *Geophysical Research Letters*, *44*(10), 4649–4659. https://doi.org/10.1002/2017gl073160

Wicht, J., & Gastine, T. (2020). Numerical simulations help revealing the dynamics underneath the clouds of Jupiter. *Nature Communications*, *11*(1), 2886. https://doi.org/10.1038/s41467-020-16680-

Wicht, J., Gastine, T., & Duarte, L. D. V. (2019). Dynamo action in the steeply decaying conductivity region of Jupiter-like dynamo models. *Journal of Geophysical Research: Planets*, *124*(3), 837–863. Retrieved from https://agupubs.onlinelibrary.wiley.com/doi/abs/10.1029/2018JE005759. https://doi.org/10.1029/2018je005759

Yu, Z. J., Leinweber, H. K., & Russell, C. T. (2010). Galileo constraints on the secular variation of the Jovian magnetic field. *Journal of Geophysical Research*, *115*(E3). https://doi.org/10.1029/2009JE003492

References From the Supporting Information

Alken, P., Thebault, E., Beggan, C. D., Aubert, J., Baerenzung, J., Brown, W. J., …Wardinski, I. (2021). Evaluation of candidate models for the 13th generation international geomagnetic reference field. *Earth Planets and Space*, *73*(1), 48. Retrieved from https://doi.org/10.1186/s40623-020-01281-4

Aubert, J., & Finlay, C. C. (2019). Geomagnetic jerks and rapid hydromagnetic waves focusing at earth's core surface. *Nature Geoscience*, *12*(5), 393–398. Retrieved from https://doi.org/10.1038/s41561-019-0355-1

Connerney, J. E. P., Benn, M., Bjarno, J. B., Denver, T., Espley, J., Jorgensen, J. L., et al. (2017). The juno magnetic field investigation. *Space Science Reviews*, *213* (1), 39–138. Retrieved from https://doi.org/10.1007/s11214-017-0334-z

Connerney, J. E. P., Timmins, S., Oliversen, R. J., Espley, J. R., Joergensen, J. L., Kotsiaros, S., et al. (2022). A new model of Jupiter's magnetic field at the completion of juno's prime mission. *Journal of Geophysical Research: Planets*, *127*(2), e2021JE007055. https://doi.org/10.1029/2021JE007055

de Boor, C. (2001). Calculation of the smoothing spline with weighted roughness measure. *Mathematical Models and Methods in Applied Sciences*, *11* (01), 33–41. https://doi.org/10.1142/S0218202501000726

Finlay, C. C., Kloss, C., Olsen, N., Hammer, M. D., Tøffner-Clausen, L., Grayver, A., & Kuvshinov, A. (2020). The chaos-7 geomagnetic field model and observed changes in the south atlantic anomaly. *Earth Planets and Space*, *72*(1), 156. https://doi.org/10.1186/s40623-020-01252-9

Langel, R. A., & Estes, R. H. (1982). A geomagnetic field spectrum. *Geophysical Research Letters*, *9*(4), 250–253. https://doi.org/10.1029/GL009i004p00250

Langlais, B., Amit, H., Larnier, H., Thébault, E., & Mocquet, A. (2014). A new model for the (geo)magnetic power spectrum, with application to planetary dynamo radii. *Earth and Planetary Science Letters*, *401*, 347–358. https://doi.org/10.1016/j.epsl.2014.05.013

Lowes, F. J. (1966). Mean-square values on sphere of spherical harmonic vec-tor fields. *Journal of Geophysical Research*, *71* (8), 2179. https://doi.org/10.1029/JZ071i008p02179

McLeod, M. G. (1996). Spatial and temporal power spectra of the geomagnetic field. *Journal of Geophysical Research*, *101*(B2), 2745–2763. https://doi.org/10.1029/95JB03042

Ridley, V. A., & Holme, R. (2016). Modeling the Jovian magnetic field and its secular variation using all available magnetic field observations. *Journal of Geophysical Research: Planets*, *121* (3), 309–337. https://doi.org/10.1002/2015JE004951